LARGE CONSTELLATION DE-ORBITING WITH LOW-THRUST PROPULSION

S. Huang,[*] C. Colombo,[†] E. M. Alessi[‡], and Z. Hou[§]

This paper deals with the propulsive phase of de-orbiting phase for coplanar satellites in large constellations. The design is conducted via two layers: the first layer is to design a time-optimal deorbiting trajectory for a single satellite; the second layer is to find the optimal de-orbit timing for each satellite to start the de-orbiting in order to minimize the total transfer time as well as the inner constellation collision risk. For the first layer, two de-orbit strategies are considered: the first strategy aims at lowering the perigee; the second strategy aims at reaching a natural de-orbiting corridor. For each strategy, the quasi time-optimal steering law is developed, and the secular variations of the orbital elements are derived by using the averaging technique. For the second layer, the inner constellation collision risk is evaluated by miss distance; the optimal de-orbit timings are found for different de-orbit sequences by using a multi-objective optimization technique.

INTRODUCTION

In the recent years, many large constellations (e.g. OneWeb and Starlink) have been announced to be deployed in the Low Earth Orbits (LEO)[1,2]. These large constellations are composed of hundreds to thousands of satellites. The purpose is to provide high speed telecommunication services to the global Earth, even the most rural areas. However, with numerous satellites injected to the already congested LEO regime, a severe safety threat will be posed to the LEO environment. In order to keep the space clean and sustainably usable, large constellations must be properly removed after their end of life, and some questions are accordingly raised, such as the assessment for different end-of-life strategies and the analysis for the execution of collision avoidance maneuvers[3].

This study focuses on two technical problems to be coped. First, the requirement of re-entry within 25 years is not enough for large constellations considering the satellites will be decommissioned frequently due to the satellite design lifetime; instead, the satellites must re-enter in less than five years[4] with the active disposal less than 2 years[5]. Second, there should be zero tolerance for any collision, that is to say, the collision risk must be minimized. There are three types of collision relating to satellite constellations: the collision between constellations and space debris, the

[*] PhD Student, Department of Aerospace Science and Technology, Politecnico di Milano, simeng.huang@polimi.it.
[†] Associate Professor, Department of Aerospace Science and Technology, Politecnico di Milano, camilla.colombo@polimi.it.
[‡‡] Researcher, Instituto di Fisica Applicata Nello Carrara, Consiglio Nazionale delle Ricerche, em.alessi@ifac.cnr.it.
[§] Post-Doctoral, Division of Information Science and Technology, Graduate School at Shenzhen, Tsinghua University, hzl1334123@163.com

collision between constellations and other operating spacecraft, and the collision between satellites within a constellation, referred to as inner-constellation collision. Up to now, most of the works (e.g. Ref. [5 – 7]) are focusing on the first two types, while the third type deserves equal attention given the sheer size of large constellations.

According to the plan by the OneWeb Constellation, low-thrust propulsion will be used for de-orbiting[1,4]. De-orbiting with low-thrust can be divided into two phases – propulsive phase (or active disposal) and non-propulsive phase (or passive disposal)[8]; the scope of this study is the propulsive phase.

This paper deals with the de-orbit problem for large constellations by using low-thrust propulsion, taking into consideration the J_2 perturbations and the Earth's shadow effect. The study will be conducted via two layers. The first layer is to design the minimum-time trajectories for a single satellite. The second layer is to find the optimal timing for each satellite to start its de-orbiting to minimize the total transfer time as well as the inner-constellation collision risk.

In the first layer, two de-orbit strategies are to be considered. The first strategy aims at lowering the perigee to achieve the passive re-entry under the atmospheric drag[9,10]. The second strategy aims at reaching a de-orbit corridor, that are conditions of resonance due to the Earth's oblateness and the solar radiation pressure; driven by these natural effects, the eccentricity can be passively increased by using a an augmentation device to enhance the effect of solar radiation pressure (for example the area-to-mass ratio tested in this work to achieve re-entry in less than 30 years is 1 m^2/kg) until the drag-dominated region is reached[11]. The propulsive phases of these two strategies are lowering the perigee in the first case and reaching the de-orbit corridor in the second case. The in-plane and out-of-plane quasi time-optimal steering laws will be developed for the two strategies, respectively. To reduce the high computation load caused by the long-duration low-thrust trajectories and the need to propagate the trajectories for multiple satellites in constellation with different initial conditions, the secular variations of the orbital elements are obtained by using the orbital averaging technique, which has been used in the previous works such as Ref. [12 – 14], under the assumption that all orbital elements except the true/eccentric/mean anomaly are constant over one orbital revolution.

In the second layer, the inner-constellation collision risk will be quantitatively evaluated by the orbit miss distance[15], the minimum relative distance between the satellites' orbits throughout the propulsive phase. The larger the miss distance, the lower the inner-constellation collision risk it will be. A multi-objective optimization technique will be used to minimize the total transfer time and to maximize the miss distance for the propulsive phase. As a preliminary study, this paper will deal with the de-orbit problem for coplanar satellites.

This paper is organized as follows. The dynamical model due to the low-thrust, J_2 perturbations and Earth's shadow will be given in the first section. The first layer, single satellite de-orbiting, will be solved in the second and third sections. In the second section, the in-plane and out-of-plane quasi time-optimal steering laws will be developed for Strategy I and II, respectively. In the third section, the secular variations of the orbital elements for the two strategies will be derived. The second layer, coplanar satellites de-orbiting, will be solved in the fourth section, in which the de-orbit sequences will be proposed and the multi-objective optimization problem will be formulated. In the last section, the numerical simulations for single satellite and coplanar satellites de-orbiting will be conducted and the results will be presented.

DYNAMICAL MODEL

The scope of this paper is the propulsive phase of de-orbiting, during which the atmospheric drag can be neglected compared with the low-thrust and J_2 perturbations, being at an orbit altitude above 1000 km, so the atmospheric drag will not be included in this paper.

The rates of change of the orbital elements with respect to the eccentric anomaly due to the low-thrust are given by[16]

$$
\begin{aligned}
\frac{\mathrm{d}a}{\mathrm{d}E} &= \frac{2a^3}{\mu}\left(e\sin E u_r + \sqrt{1-e^2}\,u_\theta\right) \\
\frac{\mathrm{d}e}{\mathrm{d}E} &= \frac{a^2}{\mu}\left(\left(1-e^2\right)\sin E u_r + \sqrt{1-e^2}\left(2\cos E - e - e\cos^2 E\right)u_\theta\right) \\
\frac{\mathrm{d}i}{\mathrm{d}E} &= \frac{a^2}{\mu}\left(\frac{\cos E - e}{\sqrt{1-e^2}}\cos\omega - \sin E\sin\omega\right)\left(1-e\cos E\right)u_h \\
\frac{\mathrm{d}\Omega}{\mathrm{d}E} &= \frac{a^2}{\mu\sin i}\left(\frac{\left(\cos E - e\right)}{\sqrt{1-e^2}}\sin\omega + \sin E\cos\omega\right)\left(1-e\cos E\right)u_h \\
\frac{\mathrm{d}\omega}{\mathrm{d}E} &= \frac{a^2}{\mu e}\left(\sqrt{1-e^2}\left(e-\cos E\right)u_r + \left(2-e^2-e\cos E\right)\sin E u_\theta\right) \\
&\quad - \frac{a^2}{\mu\tan i}\left(\frac{\left(\cos E - e\right)}{\sqrt{1-e^2}}\sin\omega + \sin E\cos\omega\right)\left(1-e\cos E\right)u_h
\end{aligned}
\tag{1}
$$

where, a is the semi-major axis, e is the eccentricity, i is the inclination, Ω is the right ascension of ascending node, ω is the argument of perigee, E is the eccentric anomaly, $\mu = 3.986 \times 10^5$ km^3/s^2 is the Earth's gravitational constant, and u_r, u_θ, and u_h are the components of the thrust acceleration vector in the radial, transversal and out-of-plane reference frame. In the above model, the time rate of change of the eccentric anomaly, even if we are in a perturbed problem, is approximated as the two-body-problem expression:

$$
\frac{\mathrm{d}E}{\mathrm{d}t} \approx \sqrt{\frac{\mu}{a^3}}\frac{1}{1-e\cos E} \tag{2}
$$

since the thrust acceleration is much smaller (usually $\leq 10^{-6}$ km/s^2) than the gravitational acceleration ($> 10^{-4}$ km/s^2).

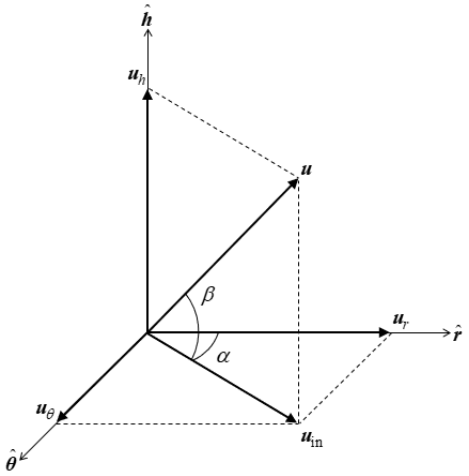

Figure 1 Thrust acceleration.

The definition of u_r, u_θ, and u_h is shown in Figure 1: u_r is the radial component, along the orbital radius vector; u_θ is the transversal component, normal to the orbital radius vector, in the orbital plane, and in the direction of the velocity; u_h is the normal component, normal to the orbital plane and along the orbital angular momentum vector. u_r, u_θ, and u_h are given by

$$\begin{aligned} u_r &= u_{\text{thrust}} \cos\alpha \cos\beta \\ u_\theta &= u_{\text{thrust}} \sin\alpha \cos\beta \\ u_h &= u_{\text{thrust}} \sin\beta \end{aligned} \tag{3}$$

where, α is the pitch angle, β is the yaw angle, u_{thrust} is the thrust acceleration magnitude, given by

$$u_{\text{thrust}} = \frac{2\eta P}{m g_0 I_{sp}} \tag{4}$$

with m being the spacecraft mass, P being the engine power, η being the engine efficiency, I_{sp} being the specific impulse and g_0 being the Earth's gravitational acceleration at sea-level.

The loss of the spacecraft mass is governed by

$$\frac{\mathrm{d}m}{\mathrm{d}t} = -m\frac{u_{\text{thrust}}}{g_0 I_{sp}} \tag{5}$$

The secular variations of the orbital elements due to the J_2 perturbations are given by[17]

$$\begin{aligned} \frac{\mathrm{d}\bar{a}}{\mathrm{d}t}_{J_2} &= \frac{\mathrm{d}\bar{e}}{\mathrm{d}t}_{J_2} = \frac{\mathrm{d}\bar{i}}{\mathrm{d}t}_{J_2} = 0 \\ \frac{\mathrm{d}\bar{\Omega}}{\mathrm{d}t}_{J_2} &= -\frac{3J_2 R_E^2}{2p^2} n\cos i \\ \frac{\mathrm{d}\bar{\omega}}{\mathrm{d}t}_{J_2} &= +\frac{3J_2 R_E^2}{4p^2} n\left(5\cos^2 i - 1\right) \end{aligned} \tag{6}$$

where, $R_E \approx 6378.16$ km is the Earth's radius, $p = a\ (1 - e^2)$ is the semi-latus rectum, and $n = \sqrt{\mu / a^3}$ is the mean motion.

The eclipses need to be considered as the low-thrust propulsion is assumed to be off in those phases. A cylindrical model for the Earth's shadow is here considered. The entry and exit eccentric anomaly of the Earth's shadow E_{en} and E_{ex} can be obtained by solving a quartic equation[18].

STEERING LAWS

The steering laws of two de-orbit strategies will be designed in this section.

Perigee Lowering Strategy

The first strategy aims at lowering the perigee. The terminal condition is given by

$$a_f \left(1 - e_f\right) = r_{p\min} \tag{7}$$

where, a_f and e_f are the semi-major axis and the eccentricity at the end of the propulsive phase, $r_{p\min}$ is the minimum perigee radius smaller than which the spacecraft will naturally re-enter.

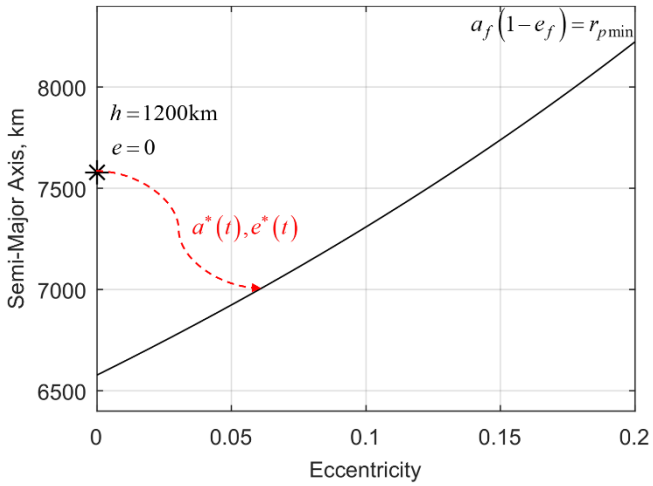

Figure 2 Interpretation on Strategy I ($r_{p\min}$ = 200 km + R_E).

Figure 2 is the graphical interpretation on Strategy I, where the asterisk indicates the OneWeb Constellation[1,4]. As shown in the figure, the objective of Strategy I is to find the quickest paths for the semi-major axis and eccentricity to reach the minimum perigee radius, represented by the black line in Figure 2. Only the in-plane thrust is needed to change the semi-major axis and eccentricity, so the yaw angle is zero, and the thrust acceleration components are given by

$$u_r = u_{\text{thrust}} \cos\alpha\ ,\ u_\theta = u_{\text{thrust}} \sin\alpha\ ,\ u_h = 0 \tag{8}$$

Noting that although only the orbital shape changes, the problem is still a three-dimensional problem.

Taking the time derivative of the perigee radius gives

$$\frac{\mathrm{d}r_p}{\mathrm{d}t} = \frac{\mathrm{d}E}{\mathrm{d}t}\left(\left(1-e\right)\frac{\mathrm{d}a}{\mathrm{d}E} - a\frac{\mathrm{d}e}{\mathrm{d}E}\right) \tag{9}$$

Under the assumption that all orbital elements except the eccentric anomaly are constant over one revolution, substituting Eqs. (1) and (2) into Eq. (9), replacing with Eq. (8), and solving for $\partial(\mathrm{d}r_p/\mathrm{d}t)/\partial\alpha = 0$ and $\partial^2(\mathrm{d}r_p/\mathrm{d}t)/\partial\alpha^2 \geq 0$ yields the local minima solution:

$$\begin{aligned}\cos\alpha &= +\frac{(1-e)^2\sin E}{\sqrt{(1-e)^4\sin^2 E+\left(1-e^2\right)\left(4\sin^2\frac{E}{2}-e\sin^2 E\right)^2}}\\ \sin\alpha &= -\frac{\sqrt{1-e^2}\left(4\sin^2\frac{E}{2}-e\sin^2 E\right)}{\sqrt{(1-e)^4\sin^2 E+\left(1-e^2\right)\left(4\sin^2\frac{E}{2}-e\sin^2 E\right)^2}}\end{aligned} \tag{10}$$

Eq. (10) is the local optimal in-plane steering law, but it is impossible to be integrated analytically even when using the orbital averaging technique. Thanks to the small eccentricity of the low Earth orbits ($e < 0.2$), it is acceptable to neglect the eccentricity while keeping the quasi optimality, and the quasi optimal in-plane steering law is given by

$$\cos\alpha = \frac{\sin E}{\sqrt{\sin^2 E+16\sin^4\frac{E}{2}}},\ \sin\alpha = -\frac{4\sin^2\frac{E}{2}}{\sqrt{\sin^2 E+16\sin^4\frac{E}{2}}} \tag{11}$$

Strategy II

The second strategy aims at reaching a de-orbit corridor. De-orbiting orbiting corridors are orbit conditions for which the eccentricity will naturally re-enter under the influence of the Earth's oblateness and solar radiation pressure enhanced by an area-augmentation device (the area-to-mass ratio tested in this work is 1 m^2/kg needed to achieve re-entry within 30 years). The terminal condition is given by

$$\left.\frac{\mathrm{d}\bar{\Omega}}{\mathrm{d}t}\right|_{J_2}\left(a_f,e_f,i_f\right)-\left.\frac{\mathrm{d}\bar{\omega}}{\mathrm{d}t}\right|_{J_2}\left(a_f,e_f,i_f\right)-n_S=0 \tag{12}$$

where, a_f, e_f, and i_f are the semi-major axis, eccentricity and inclination at the end of the propulsive phase, and $n_S \approx 2\pi/365.25$ rad/day is the motion of the longitude of the Sun measured on the ecliptic plane. Noting that this terminal condition only applies to the prograde LEO orbits of high inclination ($i \geq 77.5$ deg). For the other orbital types, one can refer to Ref. [11].

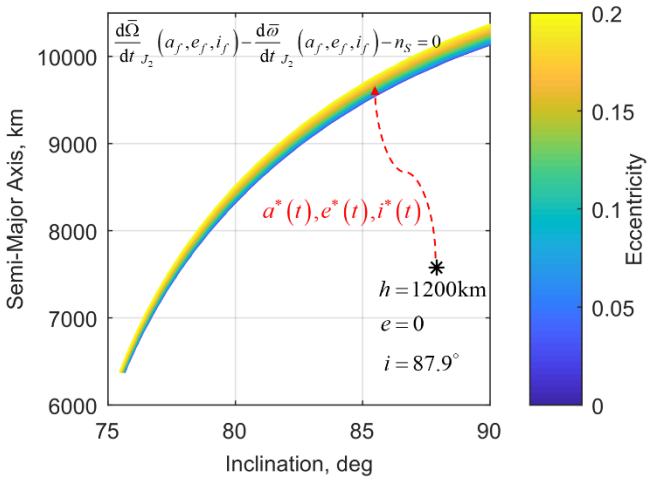

Figure 3 Interpretation on Strategy II.

Figure 3 is a graphical interpretation on Strategy II, where the asterisk indicates the OneWeb Constellation[1,4]. As shown in the figure, the objective of Strategy II is to find the quickest paths for the semi-major axis, eccentricity and inclination to reach a de-orbit corridor. For the prograde LEO orbits of high inclination (i > 77.5 deg), the semi-major axis needs to increase while the inclination needs to decrease.

The most efficient way to change the semi-major axis is via tangential thrust[19], whereas for small-eccentricity orbits, the transversal thrust is almost as efficient as the tangential thrust. The ratio of the rate of change of the semi-major axis by transversal and tangential thrust is shown in Figure 4.

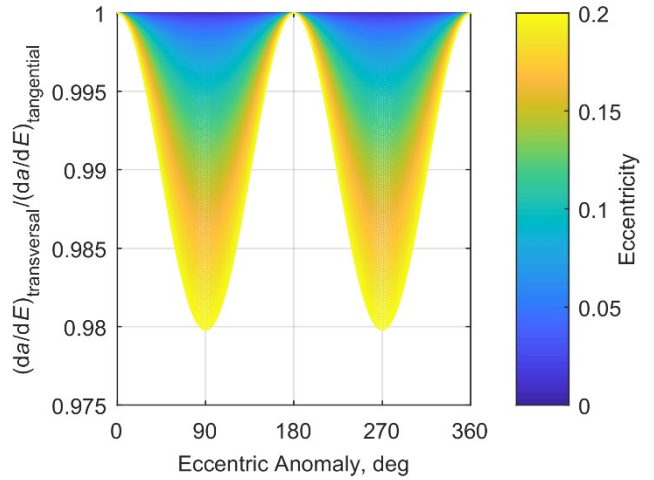

Figure 4 Ratio of da/dE by transversal and tangential thrust.

In addition, compared with tangential thrust, the dynamical model by transversal thrust is in a simpler fashion, making the integration easier when using the orbital averaging technique. From the above, this study will use the transversal thrust as the in-plane steering law, and the thrust acceleration components are given by

$$u_r = 0,\ u_\theta = u_{\text{thrust}} \cos\beta,\ u_h = u_{\text{thrust}} \sin\beta \tag{13}$$

Let us define J as.

$$J = \frac{\mathrm{d}\bar{\Omega}}{\mathrm{d}t}_{J_2} - \frac{\mathrm{d}\bar{\omega}}{\mathrm{d}t}_{J_2} - n_S \tag{14}$$

Substituting Eq. (6), after some manipulations, J can be written as

$$J = -\frac{3}{4}\sqrt{\mu} J_2 R_E^2 a^{-\frac{7}{2}} \left(1-e^2\right)^{-2} \left(5\cos^2 i + 2\cos i - 1\right) - n_S \tag{15}$$

Taking the time derivative of J gives

$$\frac{\mathrm{d}J}{\mathrm{d}t} = -\frac{3}{4}\sqrt{\mu} J_2 R_E^2 a^{-\frac{9}{2}} \left(1-e^2\right)^{-3} \frac{\mathrm{d}E}{\mathrm{d}t} \begin{pmatrix} -\frac{7}{2}\left(1-e^2\right)\left(5\cos^2 i + 2\cos i - 1\right)\frac{\mathrm{d}a}{\mathrm{d}E} \\ +4ae\left(5\cos^2 i + 2\cos i - 1\right)\frac{\mathrm{d}e}{\mathrm{d}E} \\ -2a\left(1-e^2\right)\sin i\left(5\cos i + 1\right)\frac{\mathrm{d}i}{\mathrm{d}E} \end{pmatrix} \tag{16}$$

Similar with Strategy I, under the assumption that all orbital elements except the eccentric anomaly are constant over one revolution, substituting Eqs. (1) and (2) into Eq.(16), replacing with Eq. (13), and solving for $\partial(\mathrm{d}J/\mathrm{d}t)/\partial\beta = 0$ and $\partial^2(\mathrm{d}J/\mathrm{d}t)/\partial\beta^2 \geq 0$ yields the local minima solution:

$$\cos\beta = -\frac{C_a \frac{\sqrt{1-e^2}}{1-e\cos E} + C_e \frac{e}{\sqrt{1-e^2}} \frac{2\cos E - e - e\cos^2 E}{1-e\cos E}}{\sqrt{\left(C_a \frac{\sqrt{1-e^2}}{1-e\cos E} + C_e \frac{e}{\sqrt{1-e^2}} \frac{2\cos E - e - e\cos^2 E}{1-e\cos E}\right)^2 + C_i^2 \left(\frac{\cos E - e}{\sqrt{1-e^2}}\cos\omega - \sin E \sin\omega\right)^2}}$$

$$\sin\beta = -\frac{C_i \left(\frac{\cos E - e}{\sqrt{1-e^2}}\cos\omega - \sin E\sin\omega\right)}{\sqrt{\left(C_a \frac{\sqrt{1-e^2}}{1-e\cos E} + C_e \frac{e}{\sqrt{1-e^2}} \frac{2\cos E - e - e\cos^2 E}{1-e\cos E}\right)^2 + C_i^2 \left(\frac{\cos E - e}{\sqrt{1-e^2}}\cos\omega - \sin E \sin\omega\right)^2}} \tag{17}$$

where, C_a, C_e, and C_i are given by

$$\begin{aligned} C_a &= 5.25\left(5\cos^2 i + 2\cos i - 1\right) \\ C_e &= -3\left(5\cos^2 i + 2\cos i - 1\right) \\ C_i &= 1.5\sin i\left(5\cos i + 1\right) \end{aligned} \tag{18}$$

Eq. (17) is the local optimal out-of-plane steering law, but it is impossible to be integrated analytically when using the orbital averaging technique. Same as Strategy I, neglecting the eccentricity and the quasi optimal steering law is given by

$$\cos\beta = -\frac{C_a}{\sqrt{C_a^2 + C_i^2\cos^2(\omega+E)}},\ \sin\beta = -\frac{C_i\cos(\omega+E)}{\sqrt{C_a^2 + C_i^2\cos^2(\omega+E)}} \tag{19}$$

SECULAR VARIATIONS OF ORBITAL ELEMENTS

The orbital averaging technique is used to evaluate the variations in the orbital elements per orbital revolution by integrating in the eccentric anomaly, under the assumption that all orbital elements except the eccentric anomaly are constant over one orbital revolution. The indefinite integral of the orbital element x (x can be a, e, i, Ω, or ω) can be written in the form of

$$\int \frac{\mathrm{d}x}{\mathrm{d}E}\mathrm{d}E = \mathrm{fun}_x^{\mathrm{str}*} + \mathrm{const}_x \tag{20}$$

where, fun is the primitive function, const is the integration constant, and the superscript str* indicates Strategy I or II.

For Strategy I, substituting Eq. (8) into Eq. (1), replacing with the steering law given by Eq. (11), after some manipulations, the primitive functions can be derived:

$$\begin{aligned}
\mathrm{fun}_a^{\mathrm{str1}} &= u_{\mathrm{thrust}}\frac{2a^3}{\mu}\left(\begin{array}{c}\frac{\sqrt{2}e}{3}\cos\frac{E}{2}\sqrt{5-3\cos E}\\ -\frac{4\sqrt{3}\left(3\sqrt{1-e^2}-2e\right)}{9}\tan^{-1}\frac{\sqrt{6}\cos\frac{E}{2}}{\sqrt{5-3\cos E}}\end{array}\right)\\
\mathrm{fun}_e^{\mathrm{str1}} &= u_{\mathrm{thrust}}\frac{a^2\sqrt{1-e^2}}{\mu}\left(\begin{array}{c}\frac{\sqrt{2}\left(\sqrt{1-e^2}-4+2e\cos^2\frac{E}{2}\right)}{3}\cos\frac{E}{2}\sqrt{5-3\cos E}\\ +\frac{8\sqrt{3}\left(\sqrt{1-e^2}+3e-1\right)}{9}\tan^{-1}\frac{\sqrt{6}\cos\frac{E}{2}}{\sqrt{5-3\cos E}}\end{array}\right)\\
\mathrm{fun}_i^{\mathrm{str1}} &= \mathrm{fun}_\Omega^{\mathrm{str1}} = 0\\
\mathrm{fun}_\omega^{\mathrm{str1}} &= u_{\mathrm{thrust}}\frac{a^2}{\mu e}\left(\begin{array}{c}\frac{\sqrt{2}}{3}\left(\sqrt{1-e^2}-4+e+2e^2+2e\cos^2\frac{E}{2}\right)\sin\frac{E}{2}\sqrt{5-3\cos E}\\ +\frac{2\sqrt{3}}{9}\left((4-3e)\left(1-\sqrt{1-e^2}\right)-2e^2\right)\tanh^{-1}\frac{\sqrt{6}\sin\frac{E}{2}}{\sqrt{5-3\cos E}}\end{array}\right)
\end{aligned} \tag{21}$$

where, $\tan^{-1}$ returns the four-quadrant inverse tangent, and $\tanh^{-1}$ returns the inverse hyperbolic tangent.

For Strategy II, due to the fact that there exists the term $\cos^2(\omega + E)$ in the square root of the denominator of the steering law given by Eq. (19), it is impossible to be integrated analytically. Observing that the term $\cos^2(\omega + E)$ is periodical, let us expand in two-term Fourier series before carrying out the integration:

$$\frac{1}{\sqrt{C_a^2 + C_i^2\cos^2(\omega+E)}} \approx \frac{2}{\pi\sqrt{C_a^2 + C_i^2}}\left(c_0 + c_1\cos\left(2(\omega+E)\right) + c_2\cos\left(4(\omega+E)\right)\right) \tag{22}$$

where, c_0, c_1, and c_2 are the coefficients associated with C_a and C_i, given by

$$\begin{aligned} c_0 &= ellipticF\left[\frac{C_i^2}{C_a^2+C_i^2}\right] \\ c_1 &= c_1^F\, ellipticF\left[\frac{C_i^2}{C_a^2+C_i^2}\right] + c_1^E\, ellipticE\left[\frac{C_i^2}{C_a^2+C_i^2}\right] \\ c_2 &= c_2^F\, ellipticF\left[\frac{C_i^2}{C_a^2+C_i^2}\right] + c_2^E\, ellipticE\left[\frac{C_i^2}{C_a^2+C_i^2}\right] \end{aligned} \tag{23}$$

with *ellipticF*[k] and *ellipticE*[k] being the complete elliptic integrals of the first and second kind[17]:

$$\begin{aligned} ellipticF[k] &= \int_0^{\pi/2} \frac{1}{\sqrt{1-k\sin^2\varphi}}\mathrm{d}\varphi \\ ellipticE[k] &= \int_0^{\pi/2} \sqrt{1-k\sin^2\varphi}\mathrm{d}\varphi \end{aligned} \tag{24}$$

and c_1^F, c_1^E, c_2^F, and c_2^E being the coefficients associated with C_a and C_i:

$$\begin{aligned} c_1^F &= -2\frac{2C_a^2+C_i^2}{C_i^2} \\ c_1^E &= +4\frac{C_a^2+C_i^2}{C_i^2} \\ c_2^F &= +\frac{2}{3}\frac{16C_a^4+16C_a^2C_i^2+3C_i^4}{C_i^4} \\ c_2^E &= -\frac{16}{3}\frac{2C_a^4+3C_a^2C_i^2+C_i^4}{C_i^4} \end{aligned} \tag{25}$$

Noting that the smaller the value of C_a, the more terms will be needed when carrying out the Fourier expansion. But in the present work, i.e. prograde low Earth quasi-circular orbits of high inclination (i > 77.5 deg), the two-term Fourier expansion is enough. A comparison is conducted between the left side and right side of Eq. (22) for the inclination among 77.5 deg and 90 deg in Figure 5, and it can be seen that the accuracy of the two-term Fourier expansion is acceptable.

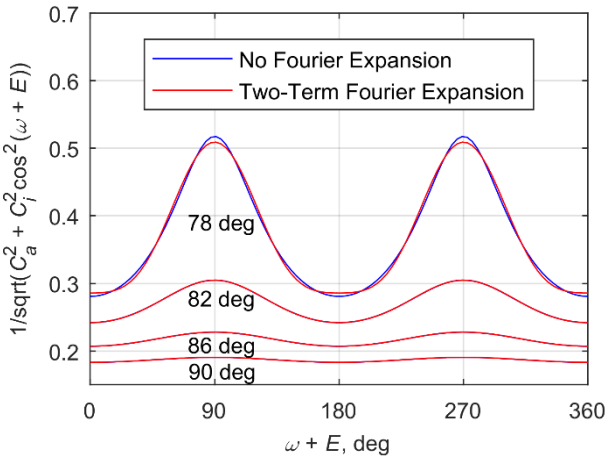

Figure 5 Accuracy of the two-term Fourier expansion.

Then substituting Eq. (13) into Eq. (1), replacing with the steering law given by Eq. (19) and the Fourier expansion given by Eq. (22), after some manipulations, the primitive functions of Strategy II can be derived:

$$
\begin{aligned}
\mathrm{fun}_a^{\mathrm{str2}} &= -u_{\mathrm{thrust}} \frac{4a^3\sqrt{1-e^2}}{\mu} \frac{C_a}{\pi\sqrt{C_a^2+C_i^2}} \left(c_0 E + \frac{1}{2} c_1 \sin\left(2(\omega+E)\right) + \frac{1}{4} c_2 \sin\left(4(\omega+E)\right) \right) \\
\mathrm{fun}_e^{\mathrm{str2}} &= -u_{\mathrm{thrust}} \frac{2a^2\sqrt{1-e^2}}{\mu} \frac{C_a}{\pi\sqrt{C_a^2+C_i^2}} \left(\boldsymbol{V}_E^e\right)^{\mathrm{T}} \left(c_0 \boldsymbol{V}_0^e + c_1 \boldsymbol{V}_1^e + c_2 \boldsymbol{V}_2^e \right) \\
\mathrm{fun}_i^{\mathrm{str2}} &= -u_{\mathrm{thrust}} \frac{2a^2}{\mu} \frac{C_i}{\pi\sqrt{C_a^2+C_i^2}} \left(\boldsymbol{V}_E^i\right)^{\mathrm{T}} \left(c_0 \boldsymbol{V}_0^i + c_1 \boldsymbol{V}_1^i + c_2 \boldsymbol{V}_2^i \right) \\
\mathrm{fun}_\Omega^{\mathrm{str2}} &= -u_{\mathrm{thrust}} \frac{2a^2}{\mu \sin i} \frac{C_i}{\pi\sqrt{C_a^2+C_i^2}} \left(\boldsymbol{V}_E^{\Omega,\omega 2}\right)^{\mathrm{T}} \left(c_0 \boldsymbol{V}_0^{\Omega,\omega 2} + c_1 \boldsymbol{V}_1^{\Omega,\omega 2} + c_2 \boldsymbol{V}_2^{\Omega,\omega 2} \right) \\
\mathrm{fun}_\omega^{\mathrm{str2}} &= -u_{\mathrm{thrust}} \frac{2a^2}{\mu} \frac{1}{\pi\sqrt{C_a^2+C_i^2}} \begin{pmatrix} \frac{C_a}{e} \left(\boldsymbol{V}_E^{\omega 1}\right)^{\mathrm{T}} \left(c_0 \boldsymbol{V}_0^{\omega 1} + c_1 \boldsymbol{V}_1^{\omega 1} + c_2 \boldsymbol{V}_2^{\omega 1} \right) \\ -\frac{C_i}{\tan i} \left(\boldsymbol{V}_E^{\Omega,\omega 2}\right)^{\mathrm{T}} \left(c_0 \boldsymbol{V}_0^{\Omega,\omega 2} + c_1 \boldsymbol{V}_1^{\Omega,\omega 2} + c_2 \boldsymbol{V}_2^{\Omega,\omega 2} \right) \end{pmatrix}
\end{aligned}
\tag{26}
$$

where, $\boldsymbol{V}_E^x$ is the column vector associated with E for the orbital element x, composed of sine and cosine terms, $\boldsymbol{V}_0^x$, $\boldsymbol{V}_1^x$, and $\boldsymbol{V}_2^x$ are the coefficient column vectors for the orbital element x, the superscript T indicates the transpose symbol. In this paper, $\boldsymbol{V}_E^x$, $\boldsymbol{V}_0^x$, $\boldsymbol{V}_1^x$, and $\boldsymbol{V}_2^x$ are not presented due to the limit of the paper length.. Note that the column vectors in $\mathrm{fun}_\Omega^{\mathrm{str2}}$ and the second part of $\mathrm{fun}_\omega^{\mathrm{str2}}$ are the same.

The variation in the orbital elements per orbital revolution should be evaluated over the orbital arcs where the spacecraft is out of the Earth's shadow. Noting that E_{en} and E_{ex} (the entry and exit eccentric anomaly of the Earth's shadow) are between 0 and 2π, so the burn arc should be $[0, E_{\mathrm{en}}]$ and $[E_{\mathrm{ex}}, 2\pi]$ if $E_{\mathrm{en}} < E_{\mathrm{ex}}$, and $[E_{\mathrm{ex}}, E_{\mathrm{en}}]$ if $E_{\mathrm{en}} > E_{\mathrm{ex}}$. Thus, the variation in the orbital element x (a, e, i, Ω, or ω) per orbital revolution due to the low-thrust propulsion is given by

$$\begin{cases} \Delta x_{\text{thrust}} = \left[\text{fun}_x^{\text{str*}} \right]_0^{E_{\text{en}}} + \left[\text{fun}_x^{\text{str*}} \right]_{E_{\text{ex}}}^{2\pi} & ,\text{if } E_{\text{en}} < E_{\text{ex}} \\ \Delta x_{\text{thrust}} = \left[\text{fun}_x^{\text{str*}} \right]_{E_{\text{ex}}}^{E_{\text{en}}} & ,\text{if } E_{\text{en}} > E_{\text{ex}} \end{cases} \tag{27}$$

Dividing by the Keplerian period $T = 2\pi/n$, the secular variation of the orbital element x (a, e, i, Ω, or ω) due to the low-thrust propulsion can be obtained:

$$\frac{\mathrm{d}\bar{x}}{\mathrm{d}t}_{\text{thrust}} = n \frac{\Delta x_{\text{thrust}}}{2\pi} \tag{28}$$

where n is the unperturbed mean motion. The total secular variation including the J_2 perturbations is given by

$$\frac{\mathrm{d}\bar{x}}{\mathrm{d}t} = \frac{\mathrm{d}\bar{x}}{\mathrm{d}t}_{\text{thrust}} + \frac{\mathrm{d}\bar{x}}{\mathrm{d}t}_{J_2} \tag{29}$$

where $\left(\mathrm{d}\bar{x}/\mathrm{d}t\right)_{J_2}$ is given by Eq. (6).

The secular variation of the spacecraft mass is given by

$$\frac{\mathrm{d}\bar{m}}{\mathrm{d}t} = n \frac{\Delta m}{2\pi} \tag{30}$$

where Δm is the mass loss per orbital revolution, given by

$$\begin{cases} \Delta m = -\dfrac{2\eta P}{g_0^2 I_{sp}^2} \dfrac{1}{n} \left(M_{\text{en}} - M_{\text{ex}} + 2\pi \right) & ,\text{if } E_{\text{en}} < E_{\text{ex}} \\ \Delta m = -\dfrac{2\eta P}{g_0^2 I_{sp}^2} \dfrac{1}{n} \left(M_{\text{en}} - M_{\text{ex}} \right) & ,\text{if } E_{\text{en}} > E_{\text{ex}} \end{cases} \tag{31}$$

with the mean anomalies M_{ex} and M_{en} being

$$\begin{aligned} M_{\text{ex}} &= E_{\text{ex}} - e \sin E_{\text{ex}} \\ M_{\text{en}} &= E_{\text{en}} - e \sin E_{\text{en}} \end{aligned} \tag{32}$$

For Strategy II, although there is a lot of trigonometric computation in the secular variations, the computation load can still be reduced a lot compared with the full dynamical integration. The comparison of the computation load will be presented in the last section of this paper.

COPLANAR SATELLITES DE-ORBITING

By implementing the quasi time-optimal steering laws and carrying out the secular variation integration, the de-orbit trajectories of a single satellite can be obtained. When extending the de-orbit problem to multiple satellites, the collision problem arises. Therefore, the objective of de-orbiting multiple satellites is not only to minimize the total transfer time but also to minimize the inner-constellation collision risk. As a preliminary study, this paper will deal with the de-orbit problem for coplanar satellites.

The total transfer time is the time from the first satellite starting de-orbiting until the last satellite meeting the terminal condition (Eq. (7) or Eq. (12)), formulated as

$$T_{\text{total}} = T_f - T_0 \tag{33}$$

where,

$$\begin{aligned} T_0 &= \min_{j=1,2,\ldots} t_0^j \\ T_f &= \max_{k=1,2,\ldots} t_f^k \end{aligned} \tag{34}$$

with t_0^j being the time of the j^{th} satellite starting de-orbiting, t_f^j being the time of the k^{th} satellite meeting the terminal condition, and N being the total number of satellites.

The inner-constellation collision risk is quantitatively evaluated by the orbit miss distance[15], the minimum relative distance between the satellites' orbits throughout the propulsive phase, formulated as

$$D_{\text{miss}} = \min_{\substack{j=1,2,\\ k=1,2,\ldots}} \left(\min_{T_0 \le t \le \min\left(t_f^j, t_f^k\right)} \Delta r^{jk}(t) \right), \quad j \neq k \tag{35}$$

where, T_0 is given by Eq. (34), Δr^{jk} is the relative distance between the j^{th} and k^{th} satellites, which can be computed by propagating the trajectories of the j^{th} and k^{th} satellites.

If we neglect the Earth's shadow effect, for not doubts it will be a good solution to let all satellites start de-orbiting at the same time. In this way the total transfer time will be the shortest and collision will not happen because the relative positions (i.e. relative phase) between the satellites are time-invariant. However, due to the introduction of the Earth's shadow effect, which can be regarded as perturbations, the relative positions will not be time-invariant and therefore collision may happen.

Take as example the OneWeb Constellation, in which there are 40 satellites per orbital plane[1,4]. If the propulsive phase for 40 satellites are to be completed in 2 years[5], then there will be on average 20 satellites to be de-orbited in each year. In order to keep the coverage performance as much as possible, it is better to keep the configuration symmetrical, as shown in Figure 6, where the red and blue points indicate the satellites to be de-orbited in the first and second year, respectively.

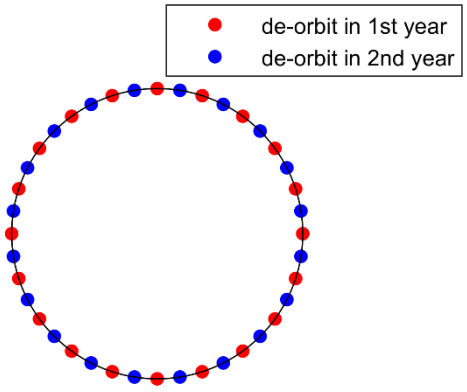

Figure 6 De-orbit sequence for 40 coplanar satellites.

In order to complete the propulsive phase for 20 satellites in one year, there are six kinds of sequence: (1) de-orbiting the satellites one by one, and finding the optimal timing for each satel-

lite; (2) de-orbiting the satellites in groups of 2, and finding the optimal timing for 10 groups; (3) de-orbiting the satellites in groups of 4, and finding the optimal timings for 5 groups; (4) de-orbiting the satellites in groups of 5, and finding the optimal timings for 4 groups; (5) de-orbiting the satellites in groups of 10, and finding the optimal timings for 2 groups; (6) de-orbiting all satellites at the same time, and no need to find the optimal timing.

Sequence (1) and (2) are safer than the others but computationally expensive when using the multi-objective optimization technique because there are 20 and 10 design variables, respectively. Sequence (5) and (6) are computationally cheaper but they are at the price of higher risk of inner-constellation collision risk because there are 10 and 20 satellites starting de-orbiting at the same time, respectively, reminding that de-orbiting multiple satellites at the same time may result in collision due to the Earth's shadow effect.

From the above, Sequence (3) and (4) are better in terms of both safety and computation load. The interpretation is shown in Figure 7, where, the points with different colors indicate the satellites from different groups, and $t_{01} - t_{05}$ are the de-orbit timings for Group 1– 5.

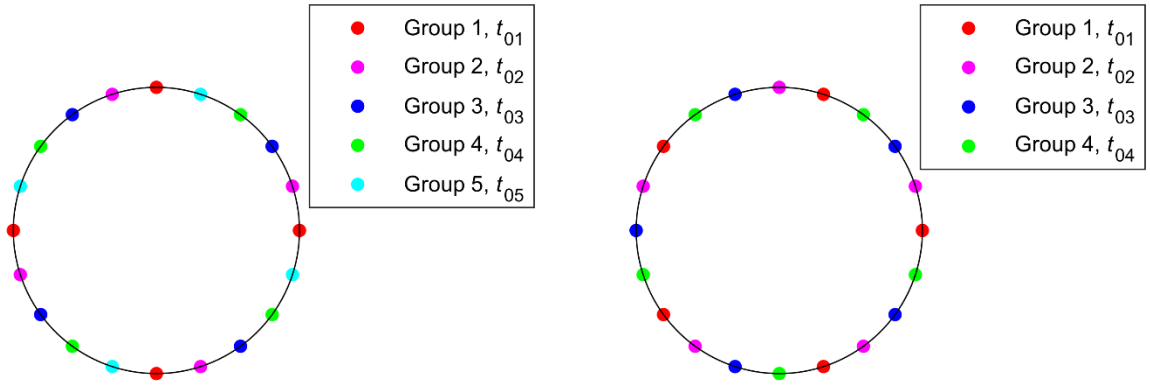

a) Sequence (3). **b) Sequence (4).**

Figure 7 De-orbit sequences for 20 coplanar satellites.

A multi-objective global optimizer is used to search for the Pareto front solutions through a multi-agent-based search approach hybridized with a domain decomposition technique developed by Vasile[20]. The cost functions of the multi-objective optimization problem are given by

$$\begin{aligned} f_1 &= \min T_{\text{total}} \\ f_2 &= -\min D_{\text{miss}} \end{aligned} \tag{36}$$

The results will be presented in the last section.

NUMERICAL SIMULATION

Two test cases are solved. In each case, the spacecraft parameters are P = 150 W, I_{sp} = 1500 s, η = 39.23%, and m_0 = 120 kg, resulting in a very small initial thrust acceleration magnitude of 6.67×10^{-8} km/s^{-2}. The initial conditions are given in Table 1. The terminal conditions for Strategy I and II are given by Eq. (7) and Eq. (12) respectively, and $r_{p\min}$ is (200 + R_E) km.

Table 1 Initial conditions.

Case	t_0	a_0 (km)	e_0	i_0 (deg)	Ω_0 (deg)	ω_0 (deg)

1	1 Sep. 2021	$1200 + R_E$	1×10^{-3}	87.9	100	200
2	1 Sep. 2022	$1200 + R_E$	1×10^{-3}	80.0	250	150

Single Satellite De-Orbiting

In the simulation for a single satellite de-orbiting, the initial true anomalies considered for Case 1 and 2 reported below are 300 deg and 50 deg, respectively. Figure 8 to Figure 10 and Figure 11 to Figure 15 present the time histories of the orbital elements for Strategy I and II, respectively. In each plot, a comparison is conducted between the full dynamical integration by local optimal steering law (black line), the full dynamical integration of the quasi optimal steering law (blue line), and the secular variation integration of the quasi optimal steering law (blue line). Here, for Strategy I and II, the local optimal steering laws are given by Eqs. (10) and (17) respectively; the quasi optimal steering laws are given by Eqs. (11) and (19) respectively, in which the eccentricity are removed from the local optimal steering laws.

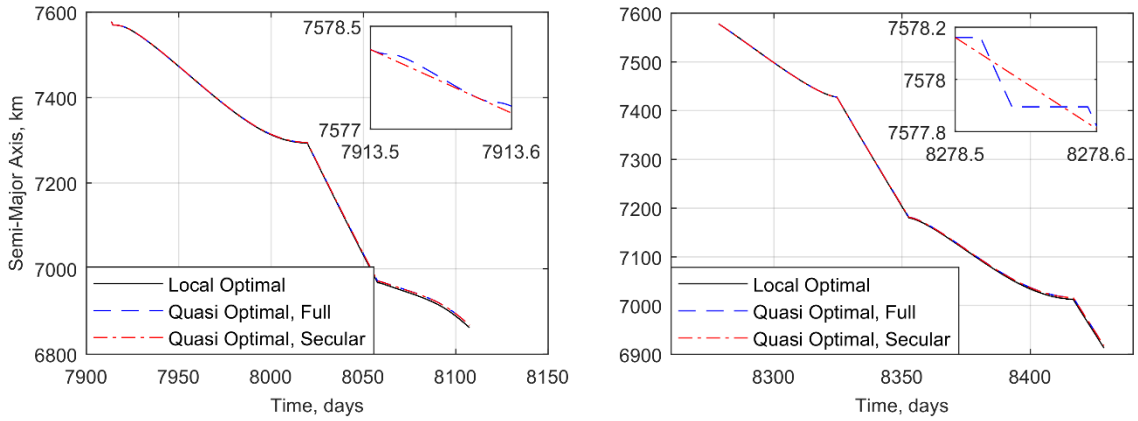

a) Case 1. **b) Case 2.**

Figure 8 Time history of the semi-major axis of Strategy I.

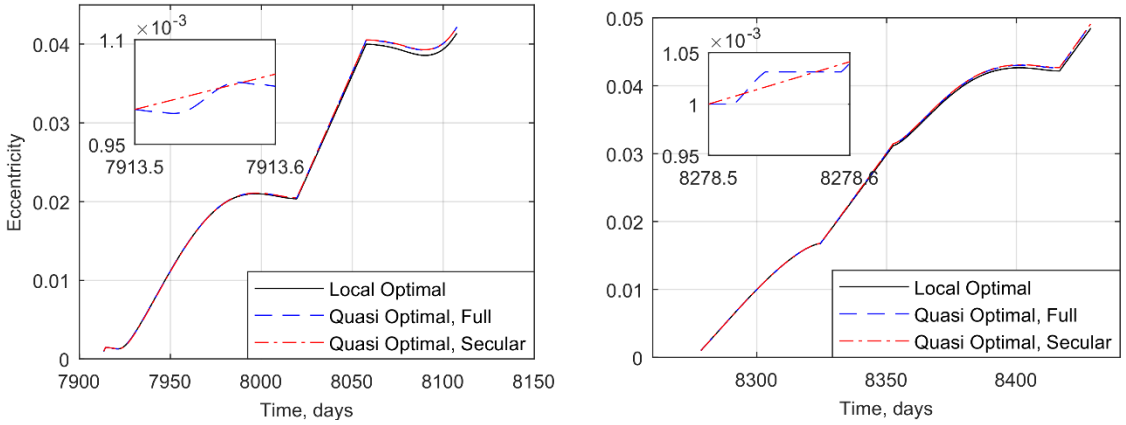

a) Case 1. **b) Case 2.**

Figure 9 Time history of the eccentricity of Strategy I.

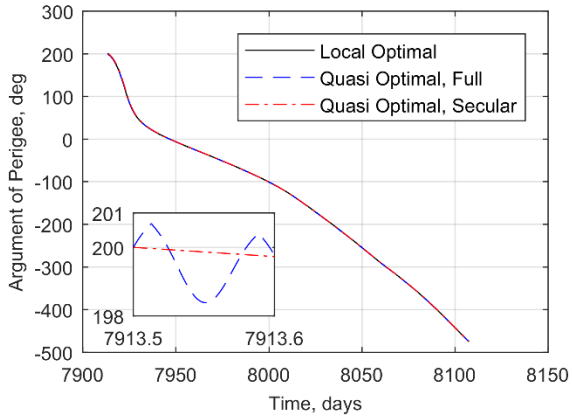

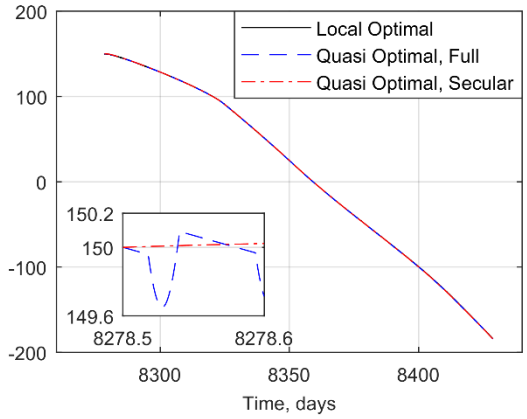

a) Case 1. **b) Case 2.**

Figure 10 Time history of the argument of perigee of Strategy I.

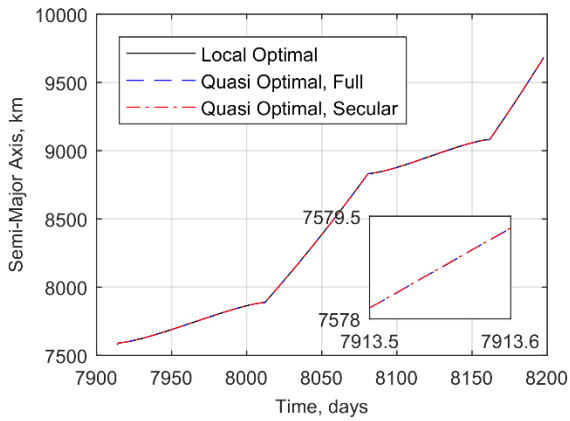

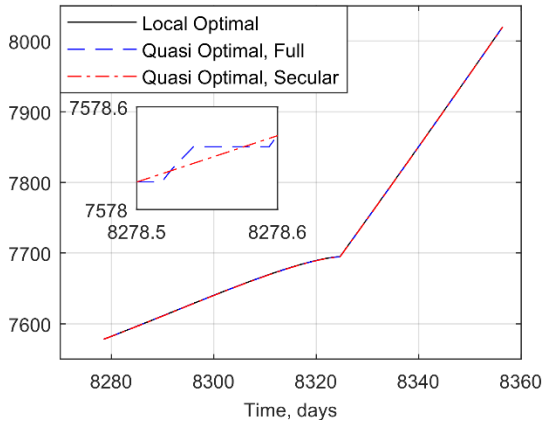

a) Case 1. **b) Case 2.**

Figure 11 Time history of the semi-major axis of Strategy II.

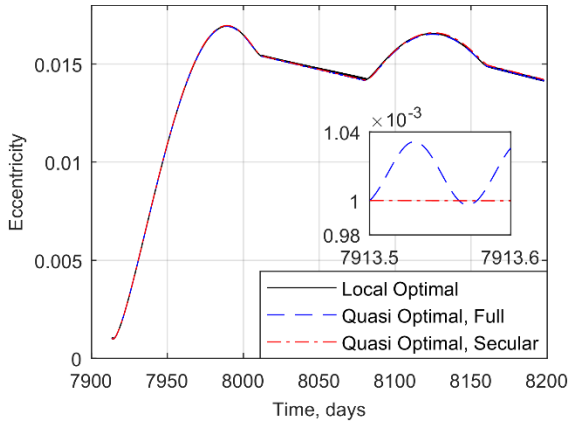

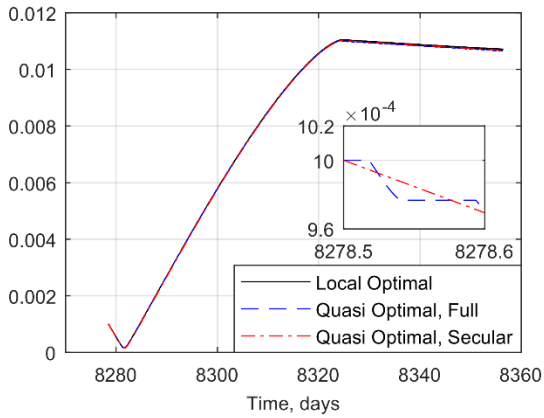

a) Case 1. **b) Case 2.**

Figure 12 Time history of the eccentricity of Strategy II.

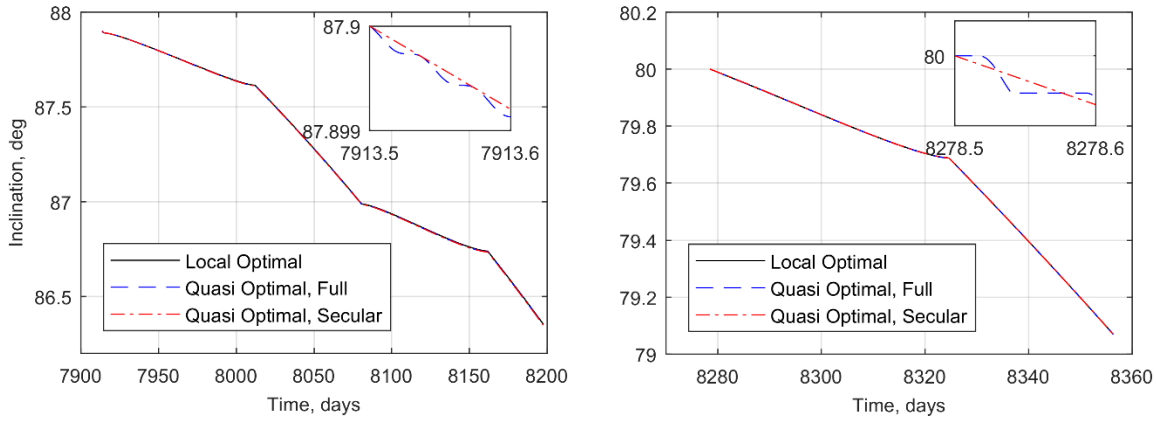

a) Case 1. **b) Case 2.**

Figure 13 Time history of the inclination of Strategy II.

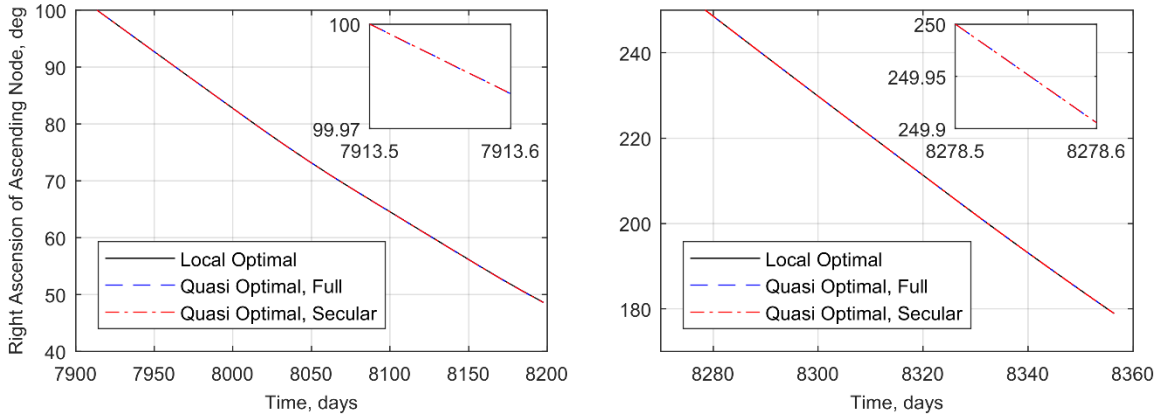

a) Case 1. **b) Case 2.**

Figure 14 Time history of the right ascension of ascending node of Strategy II.

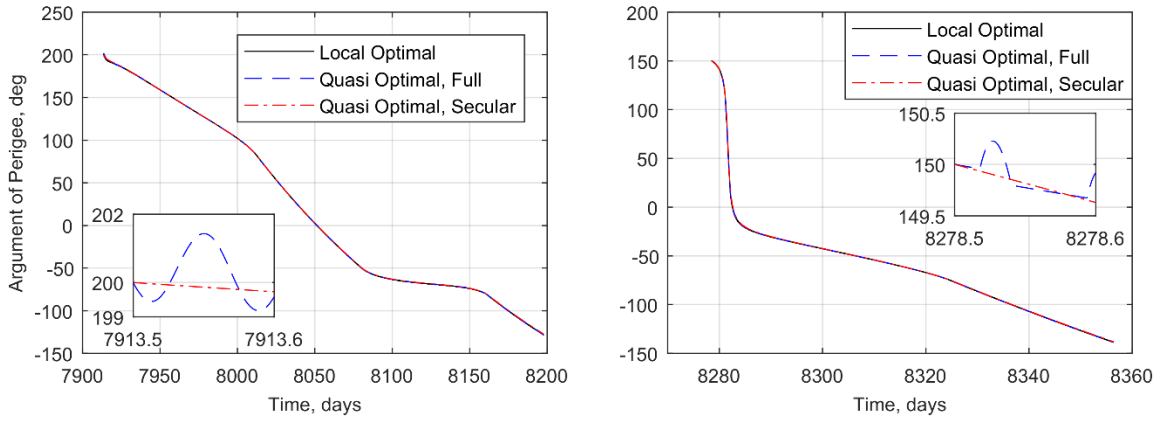

a) Case 1. **b) Case 2.**

Figure 15 Time history of the argument of perigee of Strategy II.

Table 2 and Table 3 presents the final value of the orbital elements obtained by the integration of the averaged equations using the quasi optimal steering laws for Strategy I and II, respectively.

Table 2 Final value of the orbital elements of Strategy I

Case	Strategy I					
	t_f (days)	a_f (km)	e_f	i_f (deg)	r_{pf} (km)	r_{af} (km)
1	194.03	6867.66	4.21×10^{-2}	87.9	$200 + R_E$	$778.99 + R_E$
2	150.14	6917.86	4.91×10^{-2}	87.9	$200 + R_E$	$879.40 + R_E$

Table 3 Final value of the orbital elements of Strategy II

Case	Strategy II					
	t_f (days)	a_f (km)	e_f	i_f (deg)	r_{pf} (km)	r_{af} (km)
1	284.07	9682.15	1.42×10^{-2}	86.35	$3166.38 + R_E$	$3441.60 + R_E$
2	77.89	8019.89	1.07×10^{-2}	79.07	$1556.07 + R_E$	$1727.38 + R_E$

Table 4 presents the computational time for the full dynamical and secular variation integration.

Table 4 Computational time (s)

Case	Strategy I		Strategy II	
	Full	Secular	Full	Secular
1	131.22	25.12	132.94	54.81
2	96.88	21.63	45.62	18.98

From Figure 8 to Figure 15, it can be seen that the quasi optimal steering laws for the two strategies are almost of the same efficiency as the local optimal steering laws, and the secular variation integration shows good agreement with the full dynamical integration. Besides, it can be seen from Table 4 that the computational time of the secular variation integration has been reduced compared with the full dynamical integration.

From Table 2 and Table 3, it can be seen that the de-orbiting time of Strategy I is faster than Strategy II in Case 1, whereas the de-orbiting time of Strategy II is faster than Strategy I in Case 2 (only propulsive phase). This is because the initial position of the spacecraft in Case 2 is closer to the de-orbit corridor. Therefore, a preliminary conclusion can be drawn: it is preferable to use Strategy I if the satellite initial position is far from the de-orbit corridor, and it is preferable to use Strategy II if the satellite initial position is close to the de-orbit corridor. When using Strategy II, although the total de-orbit time (i.e. including the non-propulsive phase) might be longer than by using Strategy I, Strategy II still has advantage over Strategy I in fuel consumption because the propulsive phase is shorter.

Coplanar Satellites De-Orbiting

Two sets of simulation are conducted by using Sequence (3) and Sequence (4) introduced in Figure 7. In the simulation of Sequence (3), the first de-orbit strategy is used, and the initial conditions are given by Case 1. In the simulation of Sequence (4), the second de-orbit strategy is

used, and the initial conditions are given by Case 2. In each simulation, t_{01}, the de-orbit timing of the first group of satellites, is fixed as the initial time given in Table 1. Table 5 and Table 6 give the lower and upper bounds for the de-orbit timings, in the form of the difference with respect to t_{01}. The optimization results are presented in Figure 16 to Figure 17 and Table 7 to Table 8. These results can be a reference for the management of large constellation end-of-life disposal.

Table 5 Lower and upper bounds for de-orbit timings of Sequence (3), Strategy I, Case 1

	$t_{02} - t_{01}$ (days)	$t_{03} - t_{01}$ (days)	$t_{04} - t_{01}$ (days)	$t_{05} - t_{01}$ (days)
Upper bound	30	60	90	120
Lower bound	150	150	150	150

Table 6 Lower and upper bounds for de-orbit timings of Sequence (4), Strategy II, Case 2

	$t_{02} - t_{01}$ (days)	$t_{03} - t_{01}$ (days)	$t_{04} - t_{01}$ (days)
Upper bound	15	30	45
Lower bound	75	75	75

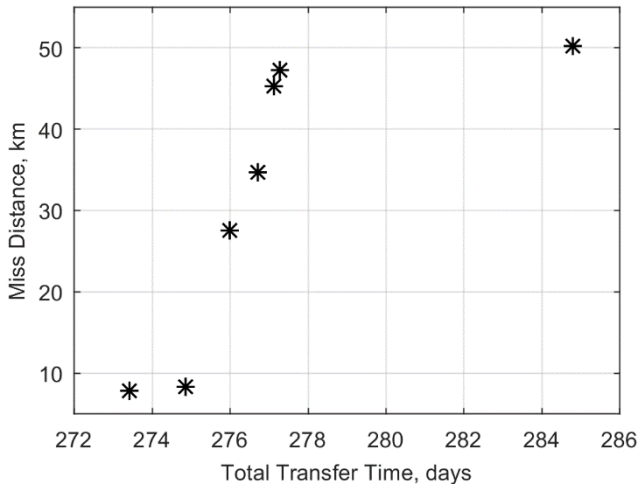

Figure 16 Optimization results of Sequence (3), Strategy I, Case 1.

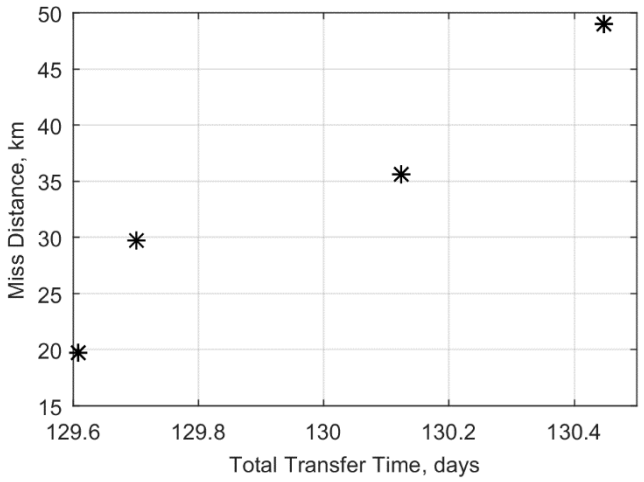

Figure 17 Optimization results of Sequence (4), Strategy II, Case2.

Table 7 Optimization results of Sequence (3), Strategy I, Case 1

$t_{02} - t_{01}$ (days)	$t_{03} - t_{01}$ (days)	$t_{04} - t_{01}$ (days)	$t_{05} - t_{01}$ (days)	T_{total} (days)	D_{miss} (km)
55.40	61.35	103.27	120	273.42	7.74
59.57	61.49	100.44	120	274.88	8.33
54.35	62.55	99.17	120.02	275.97	27.45
54.41	62.48	99.18	120	276.69	34.67
45.03	60	106.41	120.01	277.11	45.16
47.92	60	101.10	120.06	277.29	47.19
30.53	60	105.16	124.90	284.78	50.08

Table 8 Optimization results of Sequence (4), Strategy II, Case 2

$t_{02} - t_{01}$ (days)	$t_{03} - t_{01}$ (days)	$t_{04} - t_{01}$ (days)	T_{total} (days)	D_{miss} (km)
37.82	36.70	45	129.61	19.67
36.71	37.70	45	129.70	29.69
37.13	43.48	46.23	130.12	35.61
19.10	40.90	45	130.45	49.03

CONCLUSION

This paper deals with the propulsive phase of de-orbiting for coplanar satellites in large constellations. The objectives of this study is to minimize the total transfer time as well as the inner-constellation collision risk. The study is conducted via two layers: the first layer designs the trajectories for a single satellite; the second layer finds the optimal de-orbit timing for each satellite.

In the first layer, two de-orbit strategies are considered: the first strategy aims at lowering the perigee; the second strategy aims at reaching the de-orbit corridor where natural re-entry is achieved through enhancement of natural perturbations. The in-plane and out-of-plane quasi time-optimal steering laws are developed for Strategy I and II, respectively. The secular variations of the orbital elements are derived by using the orbital averaging technique. In the second layer, the inner-constellation collision risk is evaluated by the miss distance, and the multi-objective problem is formulated as minimizing the total transfer time and maximizing the miss distance.

Taking as example the OneWeb Constellation, the de-orbit sequences for coplanar satellites is proposed. The numerical simulation is conducted for both layers. For the first layer, i.e., single satellite de-orbiting, the quasi optimal steering laws are verified to have almost of the same efficiency as the local optimal steering laws, and the secular variation integration shows good agreement with the full dynamical integration, while the computation load by secular integration is noticeably reduced. Besides, a preliminary conclusion is drawn that Strategy I would be preferable if the satellite initial position is far from the de-orbit corridor, otherwise Strategy II would be preferable. For the second layer, i.e. coplanar satellites de-orbiting, the optimization results (de-orbit timings, total transfer time, and miss distance) of two different de-orbit sequences are obtained, which could be used as a reference for the management of large constellation end-of-life disposal.

In the future research, we will furtherly study the inner-constellation collision risk, trying to provide a mathematical formulization for the collision problem and to give the physical explanation for the relationship between the de-orbit timing and the orbit miss distance. In addition, this paper solves the minimum-time transfer problem by designing the time histories of pitch angle and yaw angle; for the future research, we will take into consideration the fuel consumption by designing the efficient burning arcs.

It should be noted however that Strategy II would require equipping the satellites with an area-augmentation device which might introduce higher collision hazard with the space debris. But from the constellation design point of view, since it is impossible to deploy several large constellations at the same inclination, Strategy II does has advantage over Strategy I in terms of the fuel consumption (shorter propulsive phase) at lower inclination. Besides, the augmentation device (for example in this paper the area to mass ratio is 1 m^2/kg) will not make the risk of inner-constellation collision higher compared with the orbit miss distance which will be designed larger than 5 km. In the future study, we will include the non-propulsive phase into the collision analysis and conduct a global design for large constellations, including the geometry design and the de-orbiting phase design, to minimize the inner-constellation collision risk.

ACKNOWLEDGEMENT

This project has received funding from the European Research Council (ERC) under the European Union's Horizon 2020 research and innovation programme (grant agreement No 679086 - COMPASS).

REFERENCES

[1] "Home – OneWeb | OneWorld", http://www.oneweb.world/ [retrieved 12 September 2018].

[2] "Boeing Constellation stalled, SpaceX Constellation Progressing", https://spacenews.com/boeing-constellation-stalled-spacex-constellation-progressing/ [retrived 27 June 2018].

[3] European Space Agency, "End of Life Operations for Disposal of Mega-Constellations".

[4] Lindsay, M., *OneWeb – Overview*, presentation held during the 53rd Session of the Scientific and

Technical Subcommittee of the UNCIPOUS, Ferbruary 2016.

[5] Radtke, J., Kebschull, C., and Kebschull, E., "Interactions of the Space Debris Environment with Mega Constellations-Using the Example of the OneWeb Constellation," *Acta Astronautica*, vol. 131, 2017, pp. 55–68.

[6] Chobotov, V. A., Herman, D. E., and Johnson, C. G., "Collision and Debris Hazard Assessment for a Low-Earth-Orbit Space Constellation," *Journal of Spacecraft and Rockets*, vol. 34, 1997, pp. 233–238.

[7] Swinerd, G., Lewis, H., Williams, N., and Martin, C., "Self-Induced Collision Hazard in High and Moderate Inclination Satellite Constellations," *Acta Astronautica*, vol. 54, 2004, pp. 191–201.

[8] Gaudel, A., Hourtolle, C., Goester, J. F., and Ottaviani, M., "De-Orbit Strategies with Low-Thrust Propulsion," *Space Safety is No Accident*, Springer, Cham: 2015, pp. 59–68.

[9] Pollard, J. E., "Evaluation of Low-Thrust Orbital Maneuvers," *34th Joint Propulsion Conference*, Cleveland, Ohio: 1998.

[10] Pollard, J. E., "Low-Thrust Maneuvers for LEO and MEO Missions," *35th Joint Propulsion Conference*, Los Angeles, California: 1999.

[11] Alessi, E. M., Schettino, G., Rossi, A., and Valsecchi, G. B., "Solar Radiation Pressure Resonances in Low Earth Orbits," *Monthly Notices of the Royal Astronomical Society*, vol. 473, 2017, pp. 2407–2414.

[12] Kechichian, J. A., "Orbit Raising with Low-Thrust Tangential Acceleration in Presence of Earth Shadow," *Journal of Spacecraft and Rockets*, vol. 35, 1998, pp. 516–525.

[13] Gao, Y., "Near-Optimal Very Low-Thrust Earth-Orbit Transfers and Guidance Schemes," *Journal of Guidance, Control, and Dynamics*, vol. 30, 2007, pp. 529–539.

[14] Colombo, C., Vasile, M., and Radice, G., "Semi-Analytical Solution for the Optimal Low-Thrust Deflection of Near-Earth Objects," *Journal of Guidance, Control, and Dynamics*, vol. 32, 2009, pp. 796–809.

[15] Lang, T. J., "A Comparison of Satellite Constellations for Continuous Global Coverage," *Mission Design & Implementation of Satellite Constellations*, Toulouse, France: Kluwer Academic Publishers, 1997, pp. 51–62.

[16] Pollard, J. E., "Simplified Approach for Assessment of Low-Thrust Elliptical Orbit Transfers," *25th International Electric Propulsion Conference*, Cleveland, Ohio: 1997, pp. 979–986.

[17] Battin, R. H., *An Introduction to the Mathematics and Methods of Astrodynamics*, 1999.

[18] Neta, B., and Vallado, D., *On Satellite Umbra/Penumbra Entry and Exit Positions*, 1997.

[19] Edelbaum, T. N., "Propulsion Requirements for Controllable Satellites," *ARS Semi-Annual Meeting*, Los Angeles, Calif: 1961, pp. 1079–1089.

[20] Vasile, M., "Robust Mission Design Through Evidence Theory and Multiagent Collaborative Search," *Annals of the New York Academy of Sciences*, vol. 1065, 2005, pp. 152–173.